REPORT DOCUMENTATION PAGE

Form Approved
OMB No. 0704-0188

1. REPORT DATE

2. REPORT TYPE
Professional Paper

3. DATES COVERED

4. TITLE AND SUBTITLE

A Computational Study of Unsteady Ship Wake and Vortex Flows

5a. CONTRACT NUMBER

5b. GRANT NUMBER

5c. PROGRAM ELEMENT NUMBER

6. AUTHOR(S)

Susan Polsky
Christopher Bruner

5d. PROJECT NUMBER

5e. TASK NUMBER

5f. WORK UNIT NUMBER

7. PERFORMING ORGANIZATION NAME(S) AND ADDRESS(ES)

Naval Air Warfare Center Aircraft Division
22347 Cedar Point Road, Unit #6
Patuxent River, Maryland 20670-1161

8. PERFORMING ORGANIZATION REPORT NUMBER

9. SPONSORING/MONITORING AGENCY NAME(S) AND ADDRESS(ES)

10. SPONSOR/MONITOR'S ACRONYM(S)

11. SPONSOR/MONITOR'S REPORT NUMBER(S)

12. DISTRIBUTION/AVAILABILITY STATEMENT

Approved for public release; distribution is unlimited.

13. SUPPLEMENTARY NOTES

14. ABSTRACT

The superstructure, deck, and other features of large ships produce a variety of vortex flows generated by sharp edges and massively separated regions. These features are of importance for aircraft and other operations on and around these ships. The ability to predict the airwake over a ship can aid in the development of aircraft operating envelopes and can be used to "diagnose" airwake structures that cause some landing spots to be problematic or unusable. In additin, the ability to predict airwake could be used as a design tool to address air operations early in a ship design.

15. SUBJECT TERMS

16. SECURITY CLASSIFICATION OF:			17. LIMITATION OF ABSTRACT	18. NUMBER OF PAGES	19a. NAME OF RESPONSIBLE PERSON Susan Polsky
a. REPORT	b. ABSTRACT	c. THIS PAGE			19b. TELEPHONE NUMBER (include area code)
Unclassified	Unclassified	Unclassified	SAR	7	(3)1 342-8575

Standard Form 298 (Rev. 8-98)
Prescribed by ANSI Std. Z39-18

A Computational Study of Unsteady Ship Wake and Vortex Flows

Susan A. Polsky[†] and Christopher W. S. Bruner[*]
Naval Air Warfare Center/Aircraft Division
Patuxent River, MD, USA

ABSTRACT

The superstructure, deck, and other features of large ships produce a variety of vortex flows generated by sharp edges and massively separated regions. These features are of importance for aircraft and other operations on and around these ships. The ability to predict the airwake over a ship can aid in the development of aircraft operating envelopes and can be used to "diagnose" airwake structures that cause some landing spots to be problematic or unusable. In addition, the ability to predict airwake could be used as a design tool to address air operations early in a ship design.

To date, wind tunnels have been used almost exclusively to predict ship airwake. The drawback of this approach is twofold. The first issue involves the size and speed of real ships in comparison with the available size and speed ranges of wind tunnels. Because the ships in question are so large, the scale factors required to build reasonably-sized wind tunnel models are generally in the 1/100th range. Because of this, the speeds required in a wind tunnel to match full scale Reynolds numbers (Re) are unattainable. Also, unsteady flow phenomena, which are of moderate frequency at full scale, are much higher frequency at wind tunnel scales, necessitating much higher sample rates to capture the unsteady nature of the flow. These unsteady features are often those of most concern to the pilot. The large-scale factors involved introduce Reynolds number and frequency scaling issues when attempting to scale to full-scale values. It can be argued that these flows are largely Reynolds number independent (this will be discussed in more detail later); however, this has not been shown conclusively, and the question of scale is never far from the forefront. Computational fluid dynamics (CFD) has been used in this work as an alternative approach to predicting ship airwake. CFD can be used to compute full-scale solutions and to obtain detailed off-body and time-accurate data.

Computational Method

The CFD solver COBALT (Ref. 1) was used for this study. COBALT is an unstructured-grid, Navier-Stokes solver that is optimized to run in a parallel environment. The code was run in laminar mode. In other words, no traditional Reynolds-average Navier-Stokes (RANS) turbulence model was applied; however, unresolved scales of turbulence were modeled using Monotone Integrated Large Eddy Simulation (MILES) (Ref. 2). MILES turbulence modeling is a form of Large Eddy Simulation (LES) that is inherent in time-accurate, flux-limiting schemes such as the one used in COBALT. The code was run with second-order accuracy in both time and space. The time step used (generally 0.01 seconds) was chosen to resolve frequencies up to 40 Hz based on the Nyquist criterion. Also, although the numerical scheme was unconditionally stable, the size of the time step was limited by the desired resolution of time accuracy.

Unstructured, hybrid grids on the order of 7 million cells were used. The hybrid grids consist of tetrahedra in the inviscid regions and prisms in the viscous layers. The solutions were started impulsively with freestream conditions everywhere. They were then run in a time-accurate mode for at least 40 seconds of real time to allow the flow to develop. The ship modeled, and U. S. LHA class ship, is shown in Fig. 1.

The full-scale LHA solutions were run on an IBM P3 using 64 processors. Each solution required at least 4000 iterations and approximately 128 hours of wall-clock time which was equivalent to approximately 8,000 hours of cpu time per solution Of the 4000 iterations, 1000 iterations were considered to be initialization and the remaining

[†] Aerospace Engineer.
[*] Presently Senior Research Scientist with Combustion Research and Flow Technology, Natl. Ctr. for Phys. Acoustics, University, MS.

3000 iterations, equivalent to 30 seconds, were considered to be the fully initialized, time-accurate solution set. The time steps were set to 0.01 seconds and 0.0025 seconds for the initialization stage and data acquisition stage respectively.

Results

The geometry for the ship, an LHA-class Navy ship that is approximately 820ft in length, is shown in Fig. 1. A photo of the actual ship is shown in Fig 1a and the CFD model is shown in Fig. 1b. There is considerable detail represented in the CFD model including the major features of the island, the deck and hull shape, the deck edge elevator, and the deck crane. The main features that have been neglected are the "yellow gear" (equipment used in daily operations) and the antenna arrays on the island. The yellow gear were neglected mainly because the various pieces of equipment are relatively small (compared to the size of the ship) and because they are not in fixed positions. The antenna arrays were mainly due to the complexity of modeling the antenna geometry.

Validation (Wind Tunnel Calculations)

Validation of CFD simulations when a code is applied to a new class of problems is always an important step. At the time of this writing, there are no full-scale data yet available with which to compare; therefore, wind tunnel data (Ref. 3) are used. The model geometry and the plane in which data were taken are shown in Fig. 2. The test article is a simplified version of an LHA at $1/120^{th}$ scale. The test article caused a significant amount of blockage in the tunnel; therefore, the CFD simulation included the tunnel walls.

The data were non-dimensionalized by the tunnel speed, 170 ft/s. A seven-hole probe was used to collect three-component velocity data. It should be noted that a seven-hole probe essentially records steady, time-averaged values of velocity. Therefore, unsteady aspects of the flow were not detected. As is discussed below, the unsteady nature of the flow and the type of data acquisition impact how the computational simulations must be conducted and post-processed, respectively.

The CFD solutions were run with second order time accuracy in order to resolve the unsteady nature of the flowfield. The solution was run for 2000 steps to initialize the flow and then time-accurate velocity data were collected over 0.022 seconds. The 0.022-second time period consisted of 1100 time steps of 2×10^{-5} seconds each. The 1100 samples of each velocity component were then averaged over time in order to compare directly with the seven-hole probe data.

Comparisons of the wind tunnel and CFD data for increasing heights off the deck are shown in Figs. 3a-3b. The data compare very well, and the major flow features such as the two deck-edge vortices are clearly indicated in the CFD data as a rapid dip and jump near y = +/-6 inches. Note that the data are not symmetric about y=0. This is due to the upstream influence of the island.

In these figures, x runs longitudinally down the ship, y runs across the ship from port to starboard, and z runs from the deck surface up. A y-value of 0 indicates the centerline of the ship. The u, v, and w components of velocity correspond to x, y, and z coordinate directions, respectively. The ship lies from approximately -6 inches to + 6 inches in y.

Time Accurate vs. Steady State CFD

It has been argued that even if a flow contains some unsteady features, a converged, steady-state CFD solution should result in a time averaged solution of the actual flowfield; however, that is not the case for this flow. The time-averaged u, v, and w velocity components for a deck height of 0.2315 inches. are plotted in Figs. 4a-c. Also plotted in these figures are the results from a converged, steady-state solution. As these figures demonstrate, the steady-state solution does not give the same results as the time-averaged solutions. More importantly, the steady-state results do not compare nearly as well to experiment as the time-averaged results. This is especially true of the v-velocity components near the ship centerline where the steady-state values are in significant error. The differences are most likely attributable to the fact that steady CFD solutions obtained using local timestepping (that is, integration with constant CFL number) are physically correct only when fully converged. An unsteady flow never achieves convergence (in the sense of a small residual): to the degree that unsteadiness plays a role in a problem, the solutions

obtained by applying local time-stepping are therefore not physical. Hence, while local timestepping is a powerful technique for steady problems, application of local time-stepping is inappropriate for problems with significant unsteadiness.

Full-scale Calculations

Reynolds Number & WOD Speed Independence

Because each time-accurate solution requires over 5 days of wall clock time to obtain 30 seconds of results, it would be nearly impossible to obtain results for every wind speed and angle that could be seen by the ship. As is discussed below, the flow changes dramatically as the wind angle changes, so there is little choice but to run a separate case for each wind angle of interest.

However, it appeared that the flowfield's structure did not change when varying the wind speed. In other words, an LHA flowfield at 330° and 15kts was the same as the flowfield at 330° and 30kts except that it was moving at half the speed.

In order to explore this phenomenon, two solutions were computed with 15- and 30-knot wind speeds. The wind angle was held constant at 330°. The solution from the 30-knot case was then scaled down to 15 knots by dividing the velocity components by a factor of two. Comparisons of velocity magnitudes between the two cases were made along the ship centerline, along a typical approach path, and across several landing spots. For all the locations examined, the profiles compared very well. As an example, the velocity magnitude along the centerline 10 ft above the deck is shown in Fig. 5. As the comparison shows, the 15 knot and 30 knot cases are nearly identical. A plot of surface pressure coefficients for a WOD of 15 knot and 30 knot at 330° are shown in Fig. 6. Again, the two flows are nearly identical.

The implication of this Re independence is that only one solution need be run for each wind angle of interest. That solution can then be scaled directly to any wind speed of interest. It is important to note, however, that this technique is limited in its range of application. If the speed is scaled too high, compressibility effects will corrupt the solution. Similarly, as the speed approaches zero, obviously the flow will look very different from that at 15 knots. Therefore, a minimum of two speeds must always be computed (the maximum and minimum speeds of interest) before scaling can be performed with confidence.

In addition, Re independence has not been demonstrated for the 0° WOD case. This case has substantially different aerodynamic characteristics than the oblique wind angles because the reattachment of the bow separation may be Re dependent. For the oblique wind cases, the flow over the ship is massively separated and there is no significant reattachment near or on the ship that could affect important near field wake characteristics. Re independence for the 0° WOD case is currently being tested and will be presented in the final version of this paper. If this case is not Re independent, then the next obvious question is "at what wind angle does Re become important."

It is very important to note that the Re variation being discussed here is only a factor of 2 (from 15 to 30 knots) – not a factor 100+ that is required to scale wind tunnel experiments. Therefore, the Re independence seen here may not hold foı wind tunnel applications. A CFD study is nearly complete addressing this issue. The results will be presented in the final paper.

WOD Variations

The full scale LHA CFD model is show in Fig. 1b. A series of 7 wind-over-deck (WOD) conditions were computed for wind angles of 0-90° and 270-360° at every 30 degrees (Fig. 7), and for wind speeds of 15 and 30 knots. A total of 70 seconds of real time was computed for each case. After examining several cases, it was determined that after 40 seconds had elapsed the flow was well established and most transients due to the impulsive start had flushed out of the domain. The remaining 30+ seconds of data were used for analysis.

The first case presented was for a WOD of 30 knots and 0°. Surface pressure contours at an instant in time are shown in Fig. 8. Much can be learned about the flow based on this figure such as the existence of a large separation at the bow indicated by the distinct low-pressure region (shown in blue). However, the truly complex nature of the flowfield is not revealed until the off-body flow is examined. Iso-surfaces of vorticity are shown in Fig. 9. The separation off the bow is much clearer in this figure. In addition, deck-edge vortices are easily seen. What is further revealed are "doughnut"-shaped features between the bow-separation and the island. In addition, the highly complex nature of the flow around and behind the island is indicated. When the solution was animated, it was found that the "doughnuts" are shed periodically from the bow separation at a frequency of approximately 2-3Hz. In addition, it appears that the shedding from the bow separation excites the deck edge vortices causing them to "bulge". The bulge in the vortex persists downstream until geometric features or other flow features disturb it. The doughnuts impinge on the island and interact with the island separation. All this feeds back into the area behind the island where the flow is highly separated and very complicated. In general, the flow behind the island is very unsteady and, thus far, no periodic features have been seen in this region.

The next case is again for a wind speed of 30 knots; however, the wind direction is now 30°. The major flow features change dramatically from the 0° case. First, the separation off the bow is almost nonexistent in the 30° case. In addition, there is a significant separation off the starboard deck edge and considerably more of the leeward island flow is separated (Fig. 10). The bow separation has been blown off the front of the ship. Since this separation was the driver to create the periodic shedding of the "doughnuts", these features do not appear in this flow. It is also shown that the starboard deck edge vortex is blown across the deck, and the port-side deck-edge vortex is detached from the deck edge and blown out over the ocean. The flow behind the island is more dramatically separated, and there does seem to be some periodic shedding off the island itself; however, this has not yet been confirmed by animating the solution.

The differences in the flow features as the wind-over-deck angle is changed is demonstrated in Fig. 11. Here, all seven WOD conditions are show from a top-view of the ship. It is easily seen how dramatically the flow field changes with changing wind angles. These flows will be explored in much greater detail in the final paper. In addition, animations of the flowfields will be presented at the meeting (assuming VHS or Powerpoint formatting difficulties can be overcome).

References

[1] W. Strang, R. Tomaro, and M. Grismer, "The Defining Methods of Cobalt$_{60}$: A Parallel, Implicit, Unstructured Euler/Navier-Stokes Flow Solver", AIAA Paper 99-0786, Jan. 1999

[2] J. Boris, F. Grinstein, E. Oran, R. Kolbe, "New Insights into Large Eddy Simulation", Fluid Dynamics Research 10 (1992) 199-228.

[3] Private communications with Kurt Long, NAWCAD, Patuxent River, MD and NASA Ames Fluid Mechanics Lab, Moffet Field, Ca., 1999.

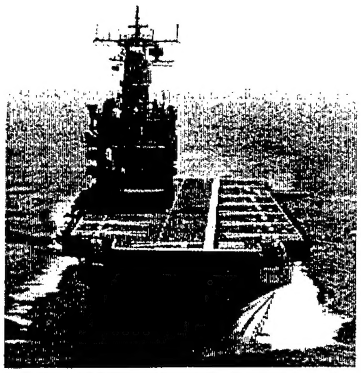

Fig 1a. LHA-2, the USS *Saipan.*

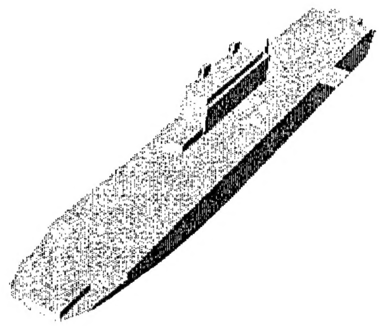

Fig 1b. CFD Model of an LHA

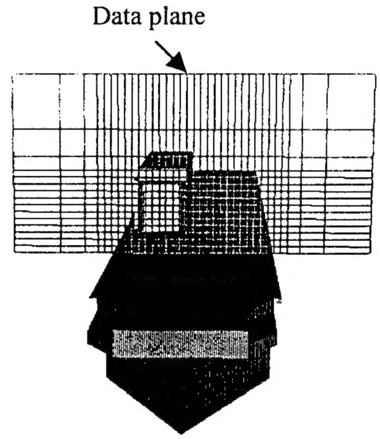

Fig 2. Wind Tunnel Model of LHA

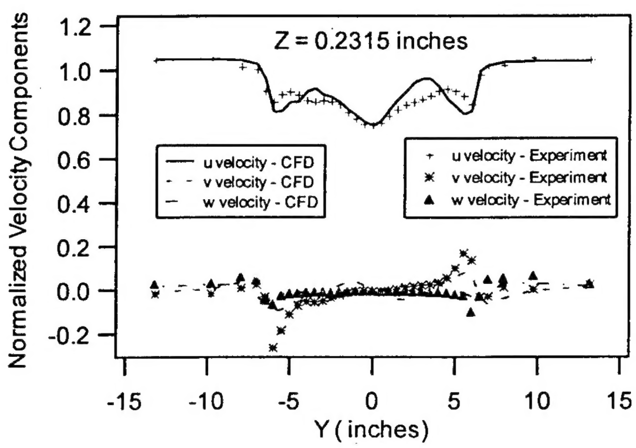

Fig 3a. Comparison of Wind Tunnel and CFD for u,v,w velocity components, Z=0.2315in.

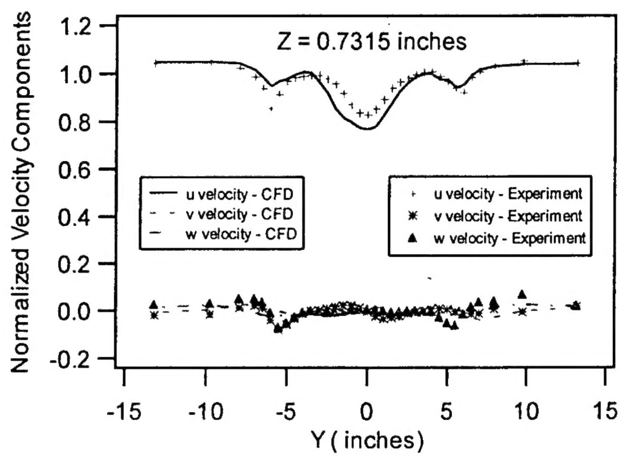

Fig 3b. Comparison of Wind Tunnel and CFD for u,v,w velocity components, Z=0.7315in.

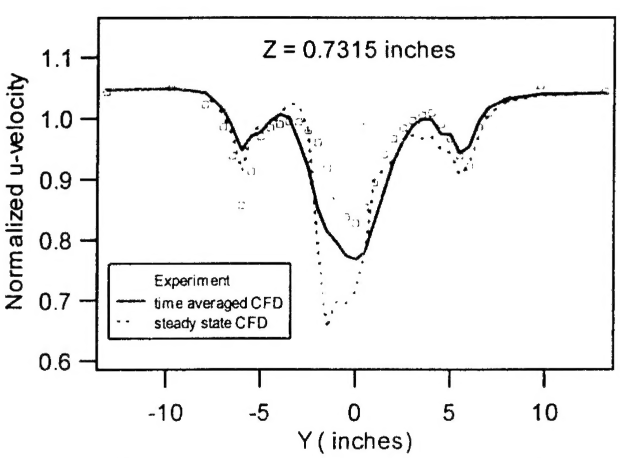

Fig 4a. Comparison of u-velocity for Wind Tunnel and CFD Data, Z=0.7315in.

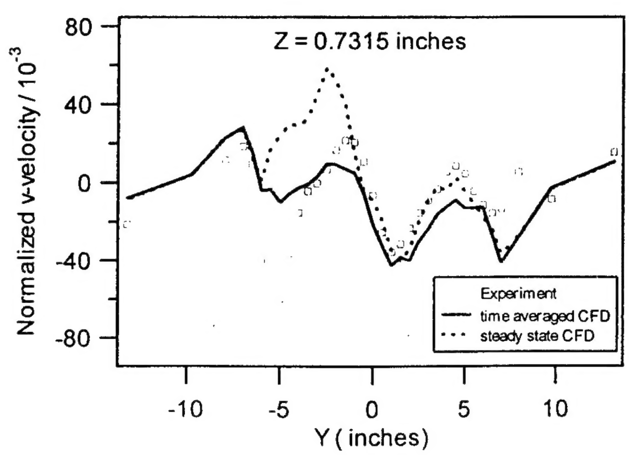

Fig 4b. Comparison of v-velocity for Wind Tunnel and CFD Data, Z=0.7315in.

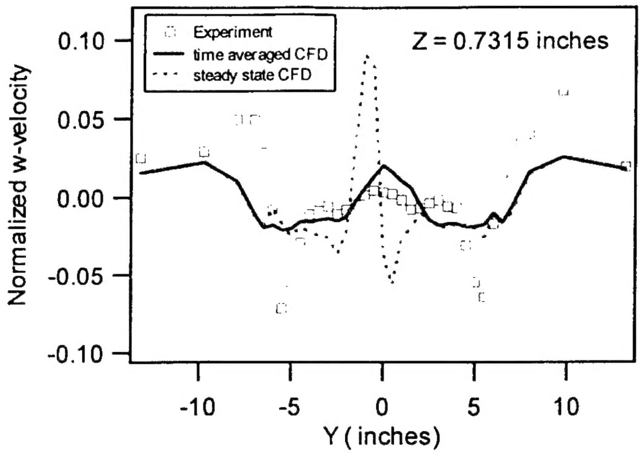

Fig 4c. Comparison of w-velocity for Wind Tunnel and CFD Data, Z=0.7315in.

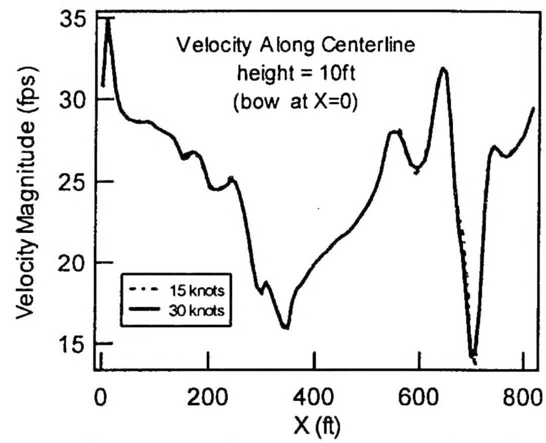

Fig 5. Centerline Velocity Comparison for Two Different Reynolds Numbers.

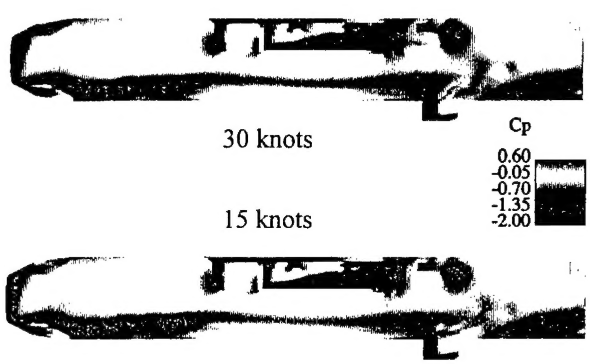

Fig 6. Surface Pressure Coefficient, Cp, for Two Different Reynolds Numbers.

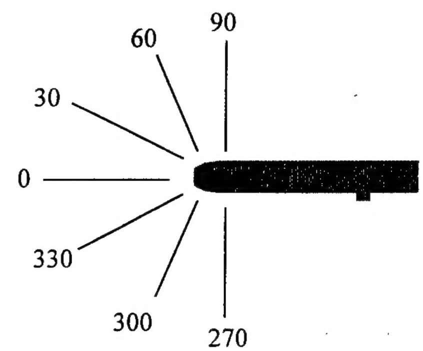

Fig 7. Wind-over-deck azimuths

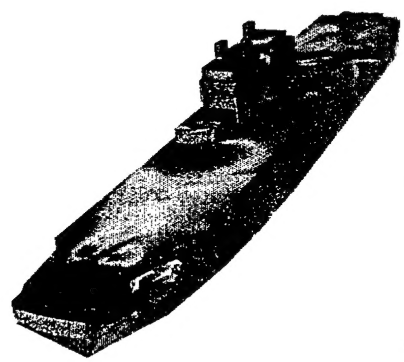

Fig 8. A Snapshot in Time of Surface pressure for WOD=0°, 30kt

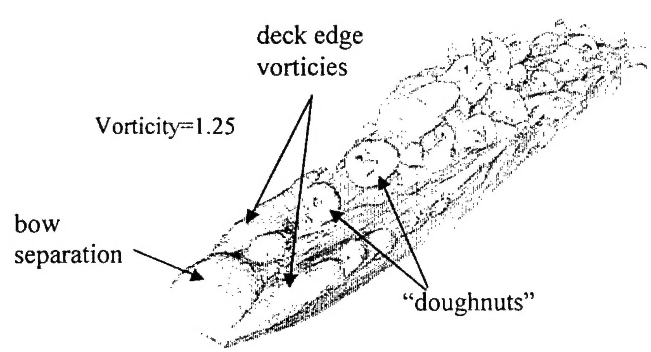

Fig 9. A Snapshot in Time of Vorticity iso-surfaces for WOD=0°, 30kt

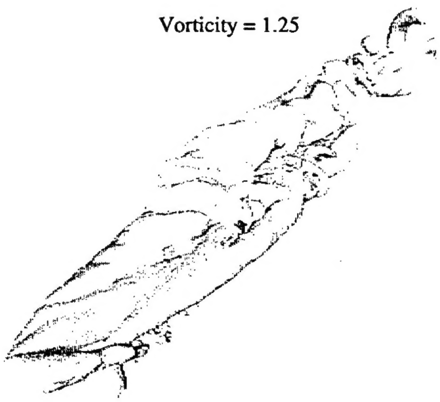

Fig 10. A Snapshot in Time of Vorticity iso-surfaces for WOD=30°, 30kt

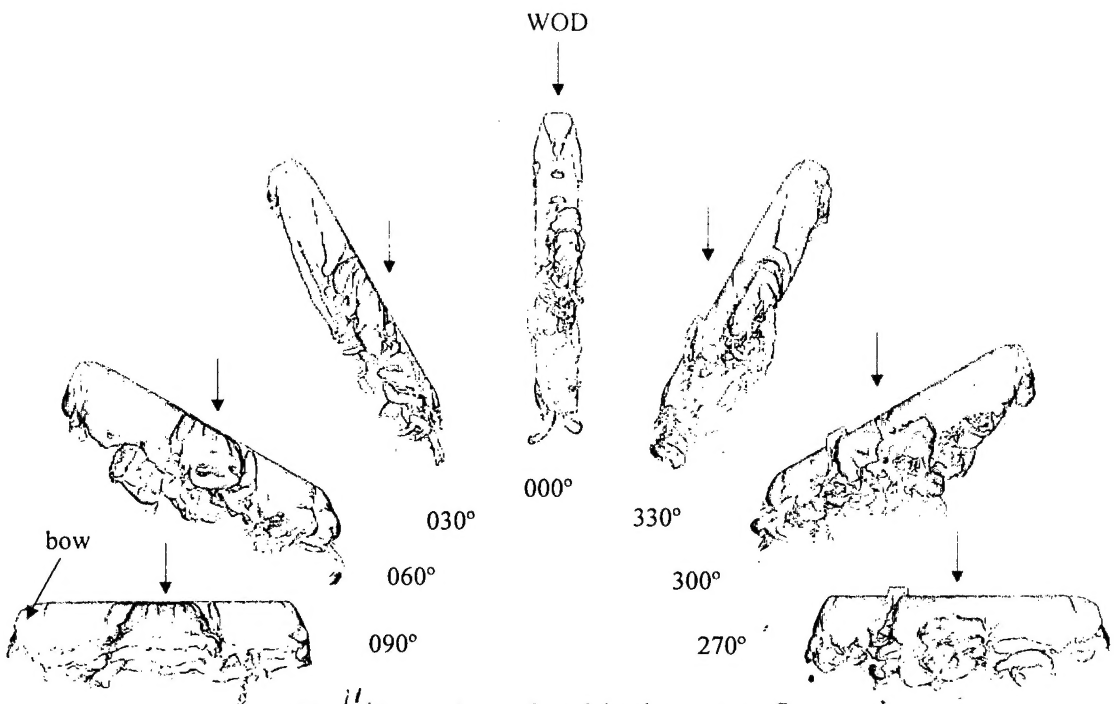

Fig 13. Iso-surfaces of vorticity demonstrate flow variations for seven WOD angles (top view, bow toward outside of figure, wind direction indicated by blue arrow.).